Hindawi
Journal of Nanomaterials
Volume 2020, Article ID 7372531, 9 pages
https://doi.org/10.1155/2020/7372531

Research Article

Antimicrobial Activity of Isoniazid in Conjugation with Surface-Modified Magnetic Nanoparticles against *Mycobacterium tuberculosis* and Nonmycobacterial Microorganisms

Sarah Zargarnezhad,[1] **Ahmad Gholami**,[2] **Mehdi Khoshneviszadeh**,[3,4] **Seyedeh Narjes Abootalebi**,[5] **and Younes Ghasemi**[1,6]

[1]*Biotechnology Research Center, Shiraz University of Medical Sciences, Shiraz, Iran*
[2]*Pharmaceutical Science Research Center, Shiraz University of Medical Sciences, Shiraz, Iran*
[3]*Department of Medicinal Chemistry, School of Pharmacy, Shiraz University of Medical Sciences, Shiraz, Iran*
[4]*Medicinal and Natural Products Chemistry Research Center, Shiraz University of Medical Sciences, Shiraz, Iran*
[5]*Division of Pediatric Intensive Care, Department of Pediatrics, Shiraz University of Medical Sciences, Shiraz, Iran*
[6]*Department of Pharmaceutical Biotechnology, School of Pharmacy, Shiraz University of Medical Sciences, Shiraz, Iran*

Correspondence should be addressed to Ahmad Gholami; gholami@sums.ac.ir

Received 6 March 2020; Revised 5 June 2020; Accepted 19 June 2020; Published 11 August 2020

Academic Editor: Ashok K. Sundramoorthy

Isoniazid, the choice antitubercular agent, has only been employed against *Mycobacterium tuberculosis*. This study evaluated if the enzyme-mimetic activities of magnetic nanoparticles could accelerate the activation process of isoniazid against mycobacterial and, more importantly, non-mycobacterial microorganisms. First, magnetic nanoparticles were synthesized and coated by lipoamino acid; then, isoniazid was conjugated to synthesized nanoparticles. Antibacterial activities of nanoconjugated isoniazid were evaluated against *Mycobacterium tuberculosis* and four Gram-positive and Gram-negative nonmycobacterial strains through a microdilution broth process. Results showed that the required amount of isoniazid against *Mycobacterium tuberculosis* would decrease to 44.8% and 16.7% in conjugation with naked and surface-modified magnetic nanoparticles, respectively. Also, 32 μg/mL and 38 μg/mL of isoniazid in conjugation with naked and surface-modified nanoparticles, respectively, could prevent the growth of *Enterococcus faecalis*, *Escherichia coli*, *Pseudomonas aeruginosa*, and *Staphylococcus aureus*. Hence, the vicinity of magnetic nanoparticles with isoniazid could declare promising aspects of isoniazid antibacterial capabilities.

1. Introduction

Despite years of investigations, tuberculosis (TB) caused by *Mycobacterium tuberculosis* (MTB) is still responsible for more than 4300 deaths every day, worldwide. The approved treatment consists of a two-phased multidrug regimen, which has faced failure in a considerable number of cases. The latest statistics of anti-TB-drug efficiency in 2017 showed that 3.5% of all new and 18% of previously treated TB patients are reported to be resistant to one or more than one of the TB drugs (MDR-TB). Furthermore, about 8.5% of these cases are categorized as extensively drug-resistant (XDR-TB) (1).

Isoniazid (INH), as an irreplaceable first-line anti-TB drug, is involved in both intensive and continuation phases of treatment (2, 3). Nevertheless, in significant cases, MTB has managed to develop resistance against it. Generally, INH is known as an antitubercular agent with no known antibacterial activity against other microorganisms. However, previous studies have linked the activated INH bactericidal activities to mechanisms (4) that could be considered quite effective against other microorganisms, as well. Theoretically, INH-derived reactive species might interfere with nonmycobacterial metabolism and growth. Hence, the question is—granting that the proper enzymatic situation is

provided—could activated INH reveal antibacterial activity against nonmycobacterial microorganisms?

Recently, the combination of antibiotics with magnetic nanoparticles (MNPs) reported promising perspectives for controlling drug-resistant infections (5, 6). Therefore, the combination of INH with these nontoxic, biocompatible materials (7, 8), could alleviate the developing resistance. MNPs also could display antibacterial activity, yet, due to unwanted oxidative effects of iron oxide on cellular structure, it is preferable to modify the particle surface by proper substances (9, 10).

In this study, a combination of INH in electrostatic interaction with lipoamino acid- (LAA-) coated MNPs (INH@smMNPs) was prepared and characterized. Then, the antibacterial activities of this nanocomplex against four gram-positive and negative pathogenic bacterial strains, including *Enterococcus faecalis*, *Staphylococcus aureus*, *Escherichia coli*, and *Pseudomonas aeruginosa* were evaluated. Also, their activity against MTB was compared with free INH.

2. Material and Methods

2.1. Synthesis of MNPs. MNPs were synthesized through the chemical coprecipitation method, using $FeCl_3{\cdot}6H_2O$ and $FeSO_4{\cdot}4H_2O$ (2 : 1 molar ratio). An aqueous solution of iron salts was stirred at 70°C under a nitrogen atmosphere. After 1 hour, 5 mL of ammonium hydroxide 32% was added until pH 11 was obtained. After another 45 minutes of stirring, black sediments were separated magnetically. Finally, precipitates were washed 4-5 times with distilled water, dried in an oven at 80°C overnight, and then kept under N_2 atmosphere at 4°C.

2.2. Synthesis of Lipoamino Acid. A total of 110 mmol of diethyl acetamidomalonate and 150 mmol of hexadecanoic bromide were dissolved in sodium with 85 mL of ethanol solution (3% *w*/*v*). The solution was refluxed at 60°C for 24 hours. The obtained precipitates were refluxed with 180 mL of HCL 1 M and 20 mL of dimethylformamide for another 24 hours. Ammonium hydroxide 32% was added to the obtained precipitates until pH 7 was gained. Finally, the resulting 2-amino-hexadecanoic acid was filtered and washed three times by absolute ethanol. The final product was kept at room temperature overnight to dry (7).

2.3. Synthesis of Surface-Modified MNPs (smMNPs). Coated MNPs were synthesized through a one-step coprecipitation method, as explained. The procedure was initiated with $FeCl_3$, $FeSO_4$, and synthetic LAA in a molar ratio of 2 : 1 : 4 in aqueous solution.

2.4. Preparation of INH Nanoconjugates. An aqueous solution of 0.3 mmol INH was added to 0.3 mmol of synthesized MNPs or smMNPs dispersed in ethanol at 40°C and stirred for 4 hours. The solution was stirred at room temperature overnight. Part of the solvent was removed under high vacuum at an external temperature of 40°C. Finally, samples were lyophilized overnight to remove residual water (11). So, INH was electrostatically attached to naked MNPs and smMNPs as INH@MNP and INH@smMNP, respectively.

2.5. Characterization of Lipoamino Acid. Synthesized LAA was characterized by FTIR spectroscopy with a KBr tablet (Bruker, Vertex 70, FTIR spectrometer) in the region of 750-4000 cm^{-1}.

2.6. Characterization of Nanocomplexes. Synthesized MNPs were characterized by FTIR spectroscopy with a KBr tablet (Bruker, Vertex 70, FTIR spectrometer), transmission electron microscopy (TEM, Zeiss, EM10C, 80 kV) graphs, vibrating sample magnetometry (VSM, LBKFB, Meghnatis Daghigh Kavir Co.), zeta potential analysis, and X-ray diffraction (XRD, Bruker, D8 Advanced, Cu-Kα) to examine the crystallinity.

2.7. Calculating Isoniazid Loaded on the Nanoparticle Surface. To evaluate the antibacterial activity of INH in comparison with its nanoconjugates, it is necessary to measure the amount of INH successfully loaded on the MNP surface. Therefore, ultraviolet spectroscopy (UV/VIS, $T80^+$) was performed, and the optical density (OD) of MNPs was compared after INH was loaded. Then, a standard curve for UV absorption of INH was drawn by Microsoft Excel 2017. The amount of INH loaded on particle surfaces was measured with the help of the acquired equation from the drawn standard curve.

2.8. Antibacterial Effect Assay. Antibacterial activities of INH against *Mycobacterium tuberculosis H37Rv*, *Enterococcus faecalis ATCC29212*, *Staphylococcus aureus ATCC29737*, *Escherichia coli ATCC15224*, and *Pseudomonas aeruginosa* ATCC9027 were evaluated by microdilution broth techniques and compared to its MNP conjugates following the method of the Clinical and Laboratory Standards Institute (12, 13).

2.8.1. In Vitro Evaluation of the Antimycobacterial Activity. The test compounds were initially dissolved in DMSO to produce a concentration of 1 μg/mL. All microplate wells received 100 μL of freshly prepared Middlebrook's 7H9 medium, except the first column. 200 μL of distilled water was added to the first column of the 96-well plates to minimize the medium evaporation in the test wells during incubation. Then, 100 μL quantities of the test compounds with the desired concentrations were added to the wells of the first row (each concentration was assayed in duplicate), and serial dilution was made from the first row to the last. A microbial suspension of 100 μL that was prepared with a standard concentration of 0.5 McFarland and diluted with a 1 : 10 proportion by distilled water was added to all the test wells. Plates were then sealed and incubated for four days at 37°C. After that, 12 μL of Tween 80 10% and 20 μL of Alamar blue 0.01% were added to each well. The plates were reincubated at 37°C. The results were assessed after 24 and 48 h.

2.8.2. In Vitro Evaluation of Antibacterial Activity against Nonmycobacterial Microorganisms. Each of the following microorganisms *Enterococcus faecalis*, *Staphylococcus aureus*, *Escherichia coli*, and *Pseudomonas aeruginosa* was suspended in freshly prepared Mueller-Hinton's broth (MBH) at a standard concentration of 0.5 McFarland and

diluted with a 1 : 20 proportion by MBH. An aqueous suspension was prepared from each of INH, INH@MNP, and INH@smMNP so that the initial concentration would contain 500 μg/mL of INH.

A 96-well microplate consisting of 45 μL culture media, 45 μL of sample (at a descending concentration of INH from 500 μg/mL to 15.625 μg/mL), and 10 μL of inoculated bacteria was applied for each microorganism. The first and last rows of the microplate were left empty to achieve a better optical contrast after plate reading. The prepared microplates were incubated for 24 hours at 37°C; then, the optical density was measured at 600 nm by a microplate reader (BioTek, PowerWave XS2). This procedure was repeated three times.

A blank 96-well microplate consisting of 45 μL of culture media and 45 μL of the sample (as explained) was prepared. At the end, 10 μL of culture media was added to each well. The turbidity of each well in a sample microplate (a microplate with the concerned microorganism) was compared to an equivalent well in a blank microplate. Microorganism viability was calculated as follows:

$$\%\text{microorganism viability} = \left(\frac{\text{OD}_{\text{bacteria+MNP}} - \text{OD}_{\text{MNP}}}{\text{OD}_{\text{bacteria}} - \text{OD}_{\text{RPMI}}}\right) \times 100. \quad (1)$$

2.9. Statistical Analysis. All antimicrobial studies were evaluated using IBM SPSS software. To determine the differences between the means of the results, the one-way ANOVA procedure and the post hoc Tukey test were performed. P value $\leq$ 0.05 was considered to be statistically significant. The experiment was repeated three times.

3. Results

3.1. Characterization. The FTIR spectra of synthesized LAA were recorded in the region of 750–4000 cm^{-1} (Figure 1). The vibrations around 1520 cm^{-1} and 3302 cm^{-1} might be related to NH band stretching and bending vibrations, respectively. The sharp peak that appeared at around 1749 cm^{-1} might be attributed to the carbonyl stretching band of carboxylic acid. Also, the stretching vibration of aliphatic C-C bands appeared at around 2940 cm^{-1}.

The FTIR spectra of the nanoconjugates of INH recorded in the region of 500-4000 cm^{-1} are shown in Figure 2. The stretching vibration of the Fe-O band around 570 cm^{-1} was able to confirm the formation of Fe_3O_4. The peak that appeared at around 1660 cm^{-1} also confirmed the existence of an acrylic carbonyl group of the INH structure. Peaks at around 3010 cm^{-1} and 3100 cm^{-1} are attributed to asymmetric and symmetric aromatic CH stretching bands, respectively, and NH stretching vibrations appeared at around 3300 cm^{-1}. In the case of INH@smMNP, the sharp peak at around 1749 cm^{-1} might be attributed to the C=O stretching bands of the LAA structure. Also, the vibrations at around 2850 cm^{-1} and 2930 cm^{-1} might be related to aliphatic stretching CH bands that exist in the LAA carbonic side chain.

TEM micrographs of drug-loaded MNPs—as shown in Figure 3—represent all spherical particles with average sizes of 11 nm and 12.93 nm for INH@MNP and INH@smMNP, respectively. To estimate the average sizes of each sample, 30 isolated particles were selected, and the mean size was reported as explained.

Hysteresis loop behavior on $0O_e$ point is shown in Figure 4 suggesting that samples caused no coercivity and remanence, which confirms their standard superparamagnetic properties. Saturation magnetization values were measured as 43.95 and 7.76 emu/g for INH@MNP and INH@smMNP, respectively.

Zeta potentials for INH@MNP and INH@smMNP were measured as +27.03 and -19.8 mV, respectively.

The X-ray pattern of the prepared compound was performed at a 2θ range of 20° to 70° at room temperature (Figure 5). Intensity peaks of INH@MNP and INH@smMNP crystallites were located at 2θ degrees of 30°, 35.5°, 43°, 57°, and 62° equivalent to (220), (311), (400), (511), and (440) Bragg reflection, respectively, which confirms the cubic spinel structure of synthesized magnetite. The peak positions were confirmed by X'Pert HighScore software. Crystallite sizes were measured by the Scherrer formula:

$$D = \frac{K\lambda}{\beta \cos\theta}, \quad (2)$$

where λ is the wavelength of X-ray radiation, which is considered 1.54 Å for all samples. β is considered as the full width at half maximum intensity at the diffracting angle. K is a constant close to unity, which is considered 0.9 when the half-width of the peak is taken. The crystallite sizes were measured as 20.80 nm and 34.66 nm for INH@MNP and INH@smMNP, respectively.

3.2. Calculation of INH Loaded on MNPs or smMNPs. The UV spectra of all samples showed the most absorption at 212 nm and 263 nm (Figure 6). Therefore, UV absorption of serially diluted concentrations of INH was read at both mentioned wavelengths. Due to Beer-Lambert's law, acquired values of optical density at 263 nm were in a more acceptable range.

Figure 7 shows the INH ultraviolet absorption standard curve with a regression value of 0.9959. Finally, according to the acquired equation, the pure amount of INH in nanocompounds was calculated, so that 1.33% of INH@MNP and 3.36% of INH@smMNP would contain pure INH.

3.3. Antibacterial Activity Evaluation

3.3.1. Antimycobacterial Activity. Minimum concentrations of pure INH, INH@MNP, and INH@smMNP for preventing more than 90% *M.T.* growth was measured as 1.26 μg/mL, 62.52 μg/mL, and 32.21 μg/mL, respectively.

3.3.2. Antibacterial Activity against Nonmycobacterial Bacteria. Acquired results showed that if antibacterial activity was compared based on INH concentration in each sample, 32 μg/mL of INH in conjugation with MNPs (as INH@MNP) or 38 μg/mL of INH in conjugation with smMNPs (as INH@smMNP) could inhibit more than

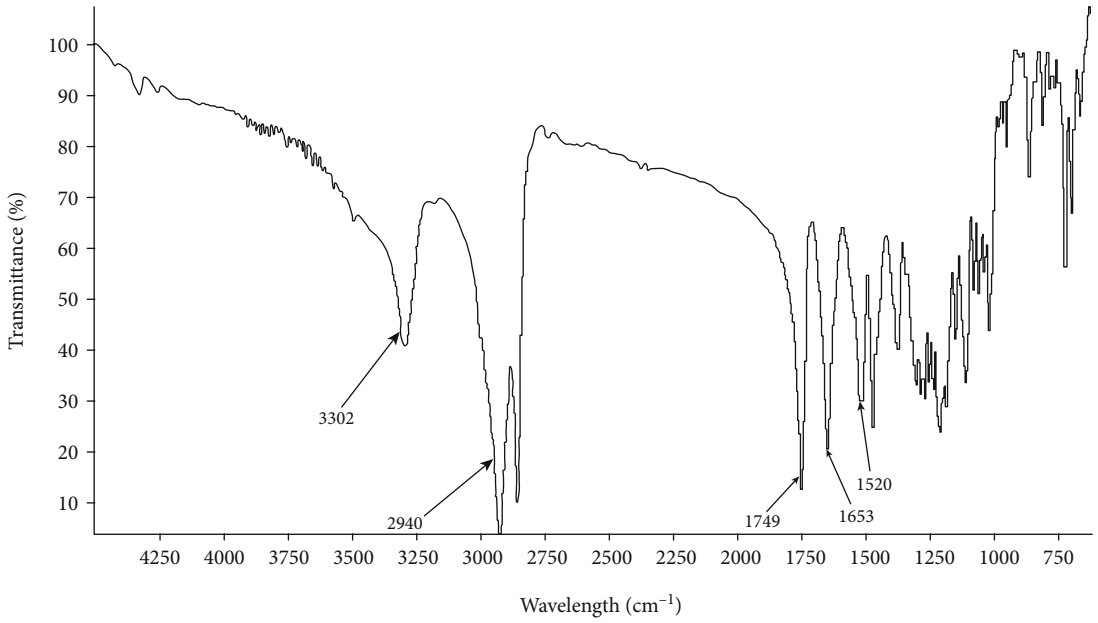

Figure 1: FTIR spectrum of lipoamino acid with a KBr tablet in the region of 750-4000 cm^{-1}.

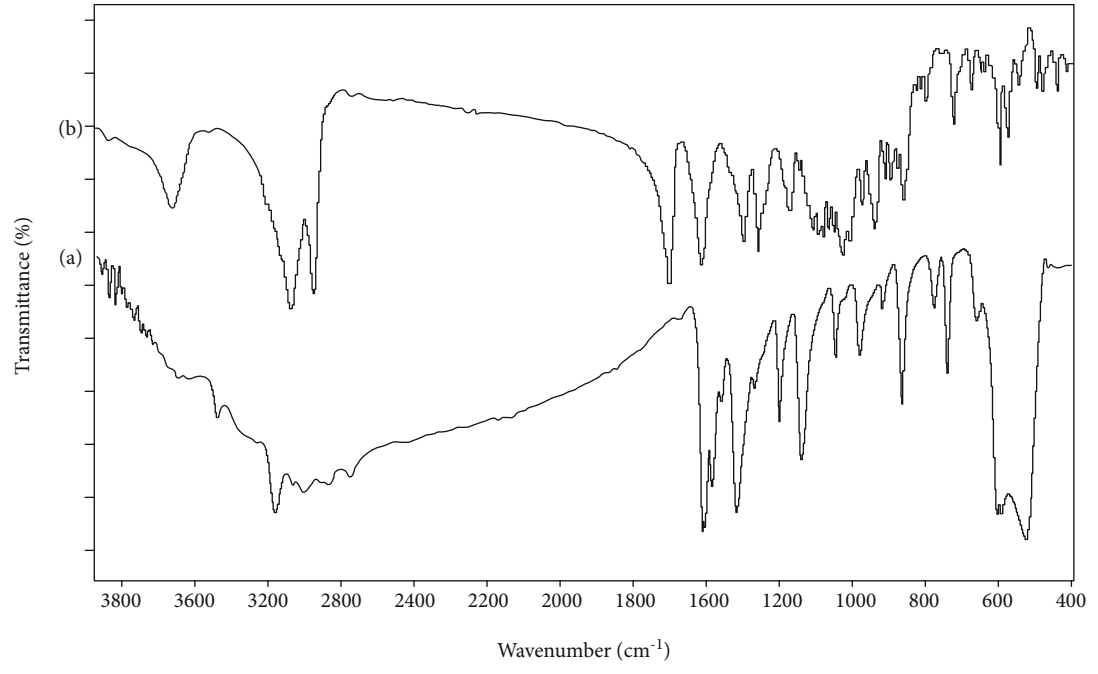

Figure 2: FTIR spectra of (a) INH@MNP and (b) INH@smMNP with a KBr tablet in the region of 500-4000 cm^{-1}.

90% of the growth of *Staphylococcus aureus*, *Escherichia coli*, and *Pseudomonas aeruginosa*. Also, 2 μg/mL of INH in conjugation with MNPs (as INH@MNP) or 9.5 μg/mL of INH in conjugation with smMNPs (as INH@smMNP) have inhibited more than 90% of the growth of *Enterococcus faecalis*. On the other hand, antibacterial activity evaluation of pure INH up to 500 μg/mL showed that the free drug is not able to efficiently prevent nonmycobacterial growth. Table 1 represents the antibacterial activity based on INH concentration in each sample.

4. Discussion

The incidence of drug-resistant TB cases is rising, as one of every three cases of TB in eastern Europe and also one of every seven cases in other areas has been reported to be resistant to INH, and the rate of this resistance is increasing every year (14). This study has focused on the resistance developed against isoniazid, one of the first-line drugs in TB treatment. Generally, INH enters the mycobacterium through the cytoplasm by passive infusion as a form of a prodrug. In the

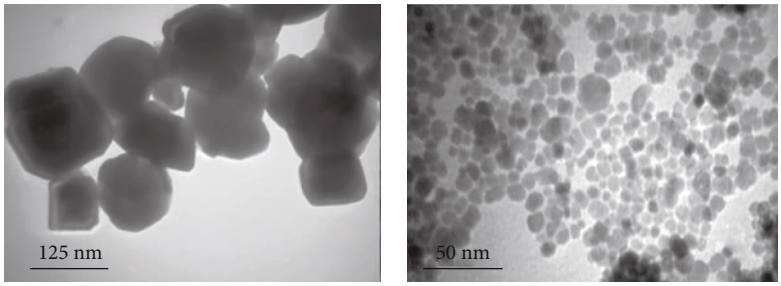

Figure 3: Transmission electron microscopy images of (a) INH@MNP and (b) INH@smMNP.

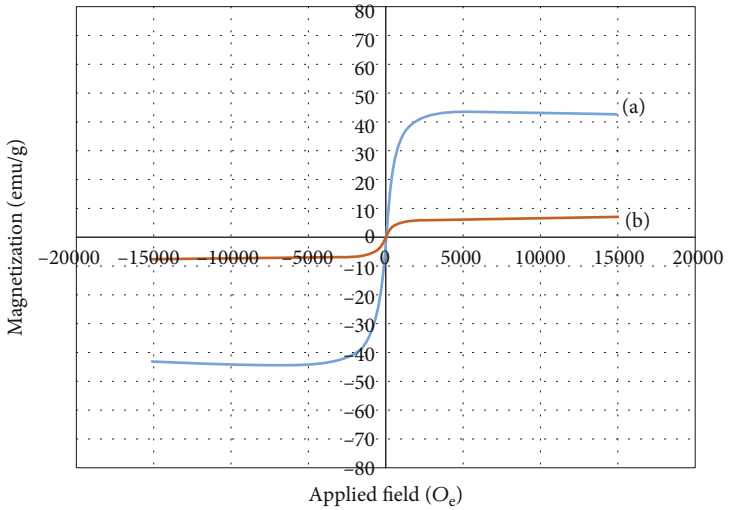

Figure 4: Magnetization curves of (a) INH@MNP and (b) INH@smMNP.

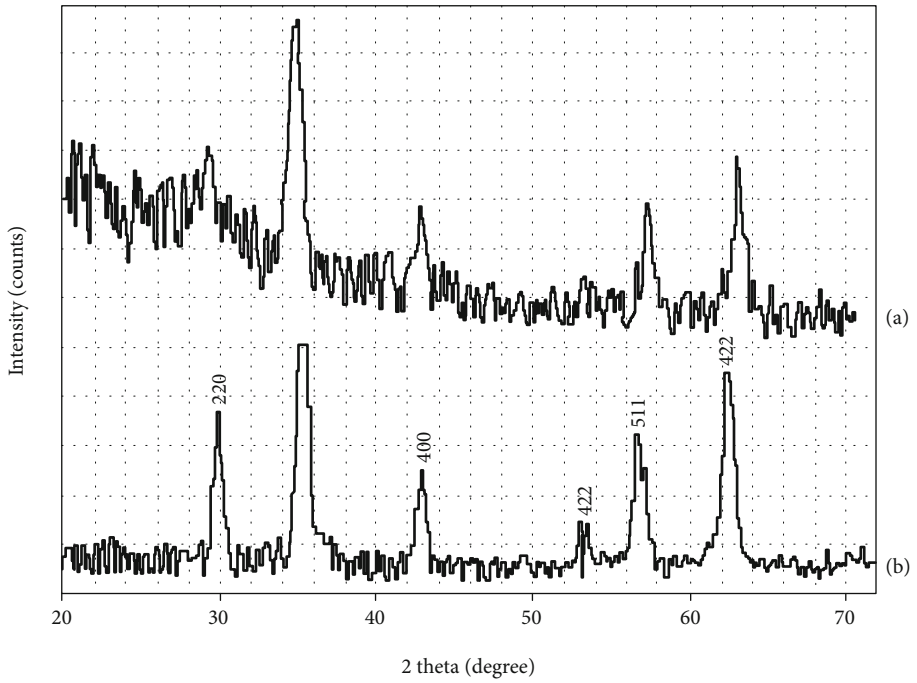

Figure 5: XRD patterns of (a) INH@MNP and (b) INH@smMNP.

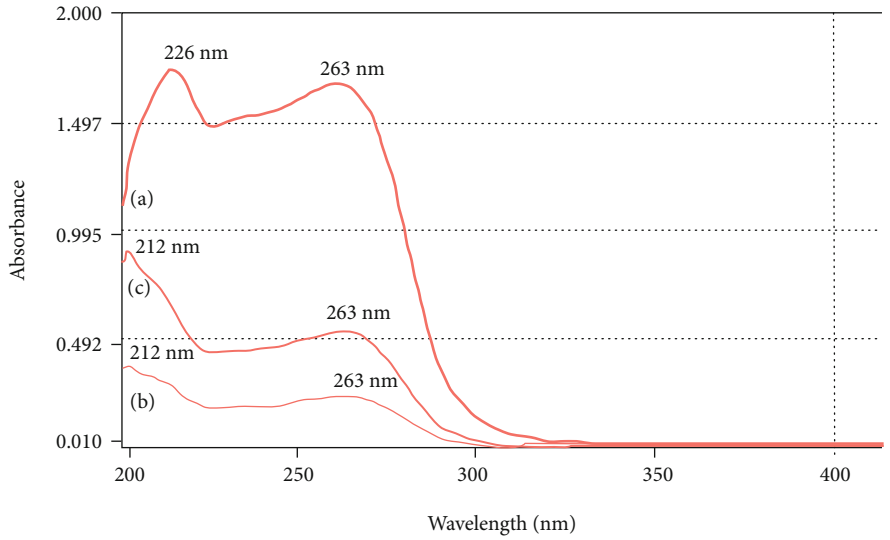

Figure 6: UV-visible absorption spectra of (a) INH, (b) INH@MNP, and (c) INH@smMNP.

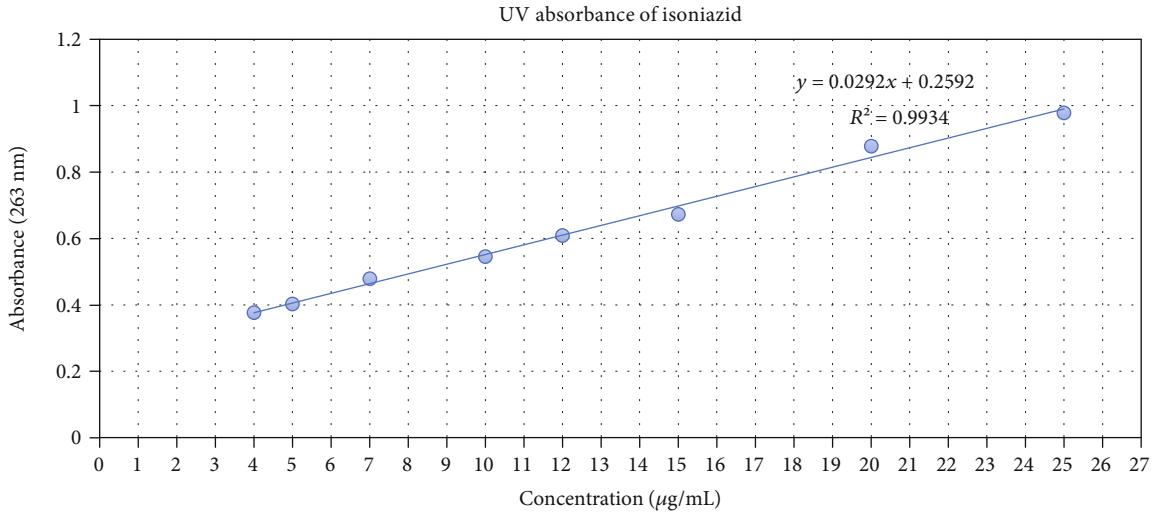

Figure 7: The standard curve of the UV-visible absorbance of INH in water.

Table 1: Antibacterial activity of nanoconjugated compounds against nonmycobacterial bacteria in comparison with pure INH.

	INH		*INH@MNP*		*INH@smMNP*	
	MIC50**	MIC90††	MIC50	MIC90	MIC50	MIC90
E. faecalis *	125	>500	2	>32	1.187	9.5
S. aureus†	>500	>500	16	>32	9.5	38
E. coli‡	500	>500	16	>32	9.5	38
P. aeruginosa§	>500	>500	16	>32	9.5	38

* *E. faecalis* = *Enterococcus faecalis*. † *S. aureus* = *Staphylococcus aureus*. ‡ *E. coli* = *Escherichia coli*. § *P. aeruginosa* = *Pseudomonas aeruginosa*. **MIC50 represents the minimum required concentration (μg/mL) of an antibacterial agent to inhibit at least 50% of bacterial growth. ††MIC90 represents the minimum required concentration (μg/mL) of an antibacterial agent to inhibit at least 90% of bacterial growth.

cytoplasm, the prodrug is affected by a multifunctional catalase-peroxidase named KatG and decomposes to the active form. The activated INH inhibits mycolic acid production, the primary material of the mycobacterial cell wall, indicating its bactericidal effect (4, 15–17).

Previous studies proved that conjugation of MNPs with antibiotics is helpful in combatting the developed resistance against antibiotics (5, 18). Also, there is a chance that in therapeutic doses, the imposition of oxidative stress by naked iron oxide NPs causes irreparable effects on mammalian cells

(7, 19). Naked MNPs, usually by adhering to the cell membrane, release reactive oxidative species (ROS) that could initiate a series of oxidation reactions leading to protein and lipid peroxidation (7, 10, 20). So far, different natural and synthetic structures have been applied to reform MNP surfaces. Nevertheless, the main feature of interest in the field of nanomaterial surface modification is not only the ability to cover the destructive effects but also the capability of drug efficiency enhancement. Previous studies on biomembrane models revealed that amphiphilic structures could cause stronger interactions with the cellular membranes. One of such materials is lipoamino acid which has been widely used in various aspects of pharmaceutical optimization (21–23). Also, the surfactant-like nature of LAAs would improve the water solubility of MNPs and prevent nanoparticle agglomeration (24, 25). Hence, the antibacterial activity of INH was compared by conjugating with naked and surface-modified MNPs.

FTIR spectra of prepared samples confirmed the presence of expected functional groups. TEM micrographs showed that all the synthesized nanoparticles were spherical. Crystalline structures of MNPs were approved by the XRD test. Also, crystalline and particle sizes of MNPs were categorized as ultra-small superparamagnetic iron oxide nanoparticles. The obtained results from VSM showed that the magnetic property of MNP-conjugated INH was considerably decreased when particle surfaces were modified by LAA, which could be probably be resolved by more optimized synthetic methods.

The utilization of MNPs in conjugation with INH showed promising improvements against MTB. According to the reported results, the minimum inhibitory concentrations of INH, INH@MNP, and INH@smMNP are equal to 1.26 μg/mL, 65.52 μg/mL, and 32.21 μg/mL, respectively. If the calculated proportion is exerted, it could be concluded that the concentrations of pure INH in INH@MNP and INH@smMNP are equivalent to 0.87 μg/mL and 1.08 μg/mL, respectively.

As mentioned previously, INH is a prodrug; when exposed to the KatG enzyme or catalase and peroxidase, it converts to the active form of the drug. A mutation in the KatG gene or the absence of catalase and peroxidase in MTBs has been listed as one of the causes that could result in INH resistance (4, 26). On the other hand, MNPs were reported to have intrinsic enzyme-mimetic properties (27, 28). Conclusively, it is expected that enzyme-mimetic activities of iron oxide NPs, specifically their peroxidase-like and catalase-like activities, have resulted in activating the prodrug. Generally, no antibacterial activity has been reported for INH, except against *Mycobacterial* strains. Nevertheless, its activity in conjugation with MNP compounds showed that the active form of the drug could be considered effective against *Enterococcus faecalis*, *Staphylococcus aureus*, *Escherichia coli*, and *Pseudomonas aeruginosa.* Thus, utilizing MNPs in the vicinity of INH has resulted in drug activation leading to the benefit of the other antibacterial mechanisms of activated INH. The activated drugs could release oxygen-, carbon-, and nitrogen-centered free radicals, which interfere with lipid, protein, and carbohydrate synthesis, and cause nucleus leakage (4).

As expected, surface modification of nanoparticles has slightly reduced the oxidative activities of iron oxide NPs. Thus, the required amount of INH against bacteria would increase when LAA is coated on nanoparticles. Despite the weaker antibacterial activity of INH@smMNP, this paper prefers to reduce the potential unintended effects of MNPs by applying surface modification. Besides, the particular amphiphilic structure of lipoamino acid could partially mimic the natural structure of the cell membrane (29, 30). Several studies have taken advantage of this characteristic to increase drug efficacy, especially antibiotics (11). Also, in the vicinity of the lung tissue (the most targeted tissue for TB), the influence of more lipophilic structures is more likely. As in the past, the use of liposomal structures was explicitly considered in the design of pharmaceutical molecules for the lung tissue (31, 32).

Khoshneviszadeh et al. showed that generally, magnetic nanoparticles display a double-edged impact on microorganism growth. So that, contrary to their antibacterial effects at therapeutic concentrations, at low concentrations (more specifically lower than 62.5 μg/mL), magnetic nanoparticles have promotive impacts on microorganism growth (8). Hence, the antibacterial effects of MNPs have been partially eliminated at the studied concentrations.

Previous investigations indicated that almost half of the TB patients could be hospitalized at least once or more during the treatment, and the average length of stay was estimated at 7-13 days or more (29). This fact would strengthen the chance of other hospital-acquired infections (HAIs). The mentioned bacteria are four of the most common causes of HAIs, which during TB treatment procedure could be easily transmitted through respiratory ventilators, infectious wounds, or pneumonia (33). Hence, the declared new aspect of INH potential utility could promise that the use of its nanoconjugates may decrease the risk of these coinfections.

5. Conclusion

Due to the resistance developed against specific drugs such as isoniazid, the treatment of tuberculosis as a serious fatal infectious disease has faced failure in a considerable number of cases. The utilization of MNPs in conjugation with INH showed promising improvements against mycobacterial and nonmycobacterial microorganisms. According to the results, the minimum inhibitory concentration of INH in conjugation with MNPs was decreased to 44.8% and 16.7% using INH@MNP and INH@smMNP, respectively. Also, antimicrobial evaluation of samples showed that at up to 500 μg/mL, pure INH revealed no inhibitory effects against nonmycobacterial strains; however, if the drug is activated, even only 32 μg/mL of INH present in INH@MNP or 38 μg/mL of INH present in INH@smMNP could already inhibit the growth of *Staphylococcus aureus*, *Escherichia coli*, and *Pseudomonas aeruginosa*. Similarly, in the case of *Enterococcus faecalis*, 2 μg/mL of INH present in INH@MNP and 9.5 μg/mL of INH present in INH@smMNP would be enough to inhibit bacterial growth. Furthermore, the conjugation of isoniazid with MNPs could not only strengthen

the antimycobacterial activity but also cause a significant antibacterial activity against nonmycobacterial strains.

Data Availability

The authors confirm that the data supporting the findings of this study are available within the article or its supplementary material.

Conflicts of Interest

The authors declare that they have no conflicts of interest.

Acknowledgments

This manuscript is based on the thesis of Sarah Zargarnezhad. The authors wish to thank the vice chancellery of Shiraz University of Medical Science for supporting this research (grant # 95-01-05-13877), and Mr. H. Argasi at the Research Consultation Center (RCC) of Shiraz University of Medical Sciences for his invaluable assistance in editing this manuscript.

Supplementary Materials

The presented image shows the antibacterial effect of the three compounds studied—isoniazid, isoniazid in conjugation with bare nanoparticles, and isoniazid in conjugation with lipoamino acid-coated SPIONs—against mycobacterial and nonmycobacterial microorganisms. *(Supplementary materials)*

References

[1] World Health O, *Global Tuberculosis Report 2013*, World Health Organization, 2013.

[2] G. Zheng, M. Wang, Q. Ren et al., "Experimental observation of mitochondrial oxidative damage of liver cells induced by isonicotinic acid hydrazide," *Experimental and therapeutic medicine*, vol. 17, no. 5, pp. 4289–4293, 2019.

[3] A. A. Agyeman and R. Ofori-Asenso, "Tuberculosis—an overview," *Public Health and Emergency*, vol. 1, 2016.

[4] G. S. Timmins and V. Deretic, "Mechanisms of action of isoniazid," *Molecular microbiology*, vol. 62, no. 5, pp. 1220–1227, 2006.

[5] A. Gholami, A. Ebrahiminezhad, N. Abootalebi, and Y. Ghasemi, "Synergistic evaluation of functionalized magnetic nanoparticles and antibiotics against Staphylococcus aureus and Escherichia coli," *Pharmaceutical nanotechnology*, vol. 6, no. 4, pp. 276–286, 2018.

[6] A. Gholami, S. Rasoul-Amini, A. Ebrahiminezhad et al., "Magnetic properties and antimicrobial effect of amino and lipoamino acid coated iron oxide nanoparticles," *Minerva Biotecnologica*, vol. 28, no. 4, pp. 177–186, 2016.

[7] A. Gholami, S. Rasoul-amini, A. Ebrahiminezhad, S. H. Seradj, and Y. Ghasemi, "Lipoamino acid coated superparamagnetic iron oxide nanoparticles concentration and time dependently enhanced growth of human hepatocarcinoma cell line (HepG2)," *Journal of Nanomaterials*, vol. 2015, Article ID 451405, 9 pages, 2015.

[8] M. Khoshneviszadeh, S. Zargarnezhad, Y. Ghasemi, and A. Gholami, "Evaluation of surface-modified superparamagnetic iron oxide nanoparticles to optimize bacterial immobilization for bio-separation with the least inhibitory effect on microorganism activity," *Nanoscience & Nanotechnology-Asia*, vol. 10, no. 2, pp. 166–174, 2020.

[9] M. J. Raee, A. Ebrahiminezhad, A. Gholami, M. B. Ghoshoon, and Y. Ghasemi, "Magnetic immobilization of recombinant E. coli producing extracellular asparaginase: an effective way to intensify downstream process," *Separation Science and Technology*, vol. 53, no. 9, pp. 1397–1404, 2018.

[10] A. Gholami, F. Mohammadi, Y. Ghasemi, N. Omidifar, and A. Ebrahiminezhad, "Antibacterial activity of SPIONs versus ferrous and ferric ions under aerobic and anaerobic conditions: a preliminary mechanism study," *IET Nanobiotechnology*, vol. 14, no. 2, pp. 155–160, 2020.

[11] R. Pignatello, A. Mangiafico, B. Ruozi, G. Puglisi, and P. M. Furneri, "Amphiphilic erythromycin-lipoamino acid ion pairs: characterization and in vitro microbiological evaluation," *AAPS PharmSciTech*, vol. 12, no. 2, pp. 468–475, 2011.

[12] A. Abbaszadegan, S. Dadolahi, A. Gholami et al., "Antimicrobial and cytotoxic activity of Cinnamomum zeylanicum, calcium hydroxide, and triple antibiotic paste as root canal dressing materials," *The journal of contemporary dental practice*, vol. 17, no. 2, pp. 105–113, 2016.

[13] A. Abbaszadegan, A. Gholami, S. Abbaszadegan et al., "The effects of different ionic liquid coatings and the length of alkyl chain on antimicrobial and cytotoxic properties of silver nanoparticles," *Iranian endodontic journal*, vol. 12, no. 4, pp. 481–487, 2017.

[14] K. Romanowski, L. Y. Chiang, D. Z. Roth et al., "Treatment outcomes for isoniazid-resistant tuberculosis under program conditions in British Columbia, Canada," *BMC infectious diseases*, vol. 17, no. 1, p. 604, 2017.

[15] P. Lempens, C. J. Meehan, K. Vandelannoote et al., "Isoniazid resistance levels of _Mycobacterium tuberculosis_ can largely be predicted by high-confidence resistance-conferring mutations," *Scientific Reports*, vol. 8, no. 1, p. 3246, 2018.

[16] S. Hu, G. Li, H. Li et al., "Rapid detection of isoniazid resistance in Mycobacterium tuberculosis isolates by use of real-time-PCR-based melting curve analysis," *Journal of clinical microbiology*, vol. 52, no. 5, pp. 1644–1652, 2014.

[17] M. N. T. Huyen, F. G. J. Cobelens, T. N. Buu et al., "Epidemiology of isoniazid resistance mutations and their effect on tuberculosis treatment outcomes," *Antimicrobial agents and chemotherapy*, vol. 57, no. 8, pp. 3620–3627, 2013.

[18] P. Bhattacharya and S. Neogi, "Gentamicin coated iron oxide nanoparticles as novel antibacterial agents," *Materials Research Express*, vol. 4, no. 9, article 095005, 2017.

[19] A. Gholami, S. M. Mousavi, S. A. Hashemi, Y. Ghasemi, W.-H. Chiang, and N. Parvin, "Current trends in chemical modifications of magnetic nanoparticles for targeted drug delivery in cancer chemotherapy," *Drug Metabolism Reviews*, vol. 52, no. 1, pp. 205–224, 2020.

[20] R. Dinali, A. Ebrahiminezhad, M. Manley-Harris, Y. Ghasemi, and A. Berenjian, "Iron oxide nanoparticles in modern microbiology and biotechnology," *Critical reviews in microbiology*, vol. 43, no. 4, pp. 493–507, 2017.

[21] S. S. Abolmaali, A. M. Tamaddon, and R. Dinarvand, "A review of therapeutic challenges and achievements of methotrexate delivery systems for treatment of cancer and rheumatoid arthritis," *Cancer Chemotherapy and Pharmacology*, vol. 71, no. 5, pp. 1115–1130, 2013.

[22] R. Pignatello, A. Leonardi, R. Pellitteri et al., "Evaluation of new amphiphilic PEG derivatives for preparing stealth lipid nanoparticles," *Colloids and Surfaces A: Physicochemical and Engineering Aspects*, vol. 434, pp. 136–144, 2013.

[23] R. A. Falconer and I. Toth, "Design, synthesis and biological evaluation of novel lipoamino acid-based glycolipids for oral drug delivery," *Bioorganic & medicinal chemistry*, vol. 15, no. 22, pp. 7012–7020, 2007.

[24] N. Ménard, N. Tsapis, C. Poirier et al., "Drug solubilization and in vitro toxicity evaluation of lipoamino acid surfactants," *International Journal of Pharmaceutics*, vol. 423, no. 2, pp. 312–320, 2012.

[25] M.-H. Wu, L.-Z. Wan, and Y.-Q. Zhang, "A novel sodium N-fatty acyl amino acid surfactant using silkworm pupae as stock material," *Scientific Reports*, vol. 4, no. 1, 2015.

[26] A. N. Unissa, S. Subbian, L. E. Hanna, and N. Selvakumar, "Overview on mechanisms of isoniazid action and resistance in Mycobacterium tuberculosis," *Infection, Genetics and Evolution*, vol. 45, pp. 474–492, 2016.

[27] L. Gao, K. Fan, and X. Yan, "Iron oxide nanozyme: a multifunctional enzyme mimetic for biomedical applications," *Theranostics*, vol. 7, no. 13, pp. 3207–3227, 2017.

[28] S. G. Kurz, J. J. Furin, and C. M. Bark, "Drug-resistant tuberculosis: challenges and progress," *Infectious Disease Clinics*, vol. 30, no. 2, pp. 509–522, 2016.

[29] K. Ronacher, N. N. Chegou, L. Kleynhans et al., "Distinct serum biosignatures are associated with different tuberculosis treatment outcomes," *Tuberculosis*, vol. 118, p. 101859, 2019.

[30] M. E. Fait, M. Hermet, F. Comelles et al., "Microvesicle release and micellar attack as the alternative mechanisms involved in the red-blood-cell-membrane solubilization induced by arginine-based surfactants," *RSC advances*, vol. 7, no. 60, pp. 37549–37558, 2017.

[31] L. Sercombe, T. Veerati, F. Moheimani, S. Y. Wu, A. K. Sood, and S. Hua, "Advances and challenges of liposome assisted drug delivery," *Frontiers in Pharmacology*, vol. 6, 2015.

[32] T. M. Allen and P. R. Cullis, "Liposomal drug delivery systems: from concept to clinical applications," *Advanced drug delivery reviews*, vol. 65, no. 1, pp. 36–48, 2013.

[33] N. Fogel, "Tuberculosis: a disease without boundaries," *Tuberculosis*, vol. 95, no. 5, pp. 527–531, 2015.